

# Volt-Ampere Ratings in Electronically-Tuned Linear Alternators for Thermo-Acoustic Engines

Matteo F. Iacchetti<sup>1\*</sup>, Roger Shuttleworth<sup>1</sup>, Min Zhang<sup>1</sup>

<sup>1</sup> School of Electrical and Electronic Engineering, University of Manchester, Manchester, U.K.

\* [matteo.iacchetti@manchester.ac.uk](mailto:matteo.iacchetti@manchester.ac.uk)

**Abstract:** Linear Alternators (LAs) coupled to Thermo-Acoustic Engines (TAEs) provide a viable solution to extract energy from a heat source in a variety of applications such as waste heat, energy harvesting, solar thermal and biomass power generation. For the electrical power to be maximized, the acoustic impedances of LA and TAE have to match. This requirement cannot in general be met by relying only on the design of the LA, but can be achieved at the control level, by using a fraction of the LA inverter current to create “electronic stiffness” which contributes to the overall stiffness tuning the resonance frequency. The same concept can in principle be used to replace part of the mechanical spring stiffness in order to overcome limitations in the mechanical design, at the expense of an increase in LA and inverter ratings. The impact of electronic stiffness on LA power capability and ratings is analysed here. Two meaningful scenarios are considered in the analysis: the LA derating for resonance frequency tuning, and the oversizing when springs are partially replaced by electronic stiffness. The study is supplemented with experiments on a small-scale LA test rig.

## 1. Introduction

Linear Alternators (LAs) are key components for enabling electrical power generation with reciprocating thermal engines such as Thermoacoustic Engines (TAEs) and Free-Piston Stirling Engines (FPSEs). TAEs, in particular, are seen as a disruptive technology for cheap and reliable waste heat recovery systems [1].

The preferred LA topology adopted with TAEs uses a moving Permanent Magnet (PM) plunger connected to a piston driven by pressure waves [1]-[3]. A similar structure is adopted in FPSEs [4]-[6], and in wave energy generation systems, where the LA plunger is directly driven by waves [7]-[8]. In some low-power TAEs, the LA can be replaced by a low-cost loudspeaker [9].

Published studies dealing with the control of LAs are mainly dedicated to wave energy conversion [10]-[14], with only a few papers specifically focusing on LA control in TAE or FPSEs [3], [15]-[16].

One of the first control schemes for a LA coupled to a single-phase 350 W FPSE was proposed in [15] using a Voltage-Source Inverter (VSI) to compensate for the internal LA impedance and then estimate the stroke from the terminal voltage. In [14] and [16], the VSI was used to maintain the current in phase with the internal EMF in three-phase LAs for FPSEs, thereby realizing a Maximum Thrust Per Ampere (MTPA) condition. This is similar to the maximum torque per ampere condition for rotating PM synchronous machines (PMSMs). The concept of having current and EMF in phase with each other was adopted in a three-phase direct-drive Vernier LA for wave energy conversion in [11], and the inverter ratings were discussed under the assumption of sinusoidal wave excitation. A similar control framework was adopted in [14] for a permanent magnet LA driven by an Archimedes wave spring.

One of the distinctive features of LA operation in these systems is the alternating variation of the plunger kinetic energy over a cycle. It is assumed here that the piston is part

of the plunger. The usual method of handling this “reactive” energy flow with minimum loss is to transiently store it in mechanical springs, realizing then a resonant mechanical system, which can be tuned to the frequency of forcing waves.

Although zero phase-shift between EMF and current maximizes the generated power per ampere for a given stroke length, mismatches between resonant and operating frequencies cause a drop in stroke length and a consequent reduction in maximum power converted [17]. The impedance matching needed to maximize power extraction can be achieved with phase and amplitude controllers for LA currents, as proposed in [12] for a three-phase LA driven by ocean waves. In theory, this control concept can be refined further, to tune reactive elements individually regardless of frequency, but the implementation becomes difficult as it requires position, speed and acceleration measurements [18].

Impedance matching is even more important in TAEs, as it also affects the onset of pressure oscillations in the engine itself [19]. The possibility of electronically changing the LA equivalent acoustic impedance seen by the pressure wave source can be exploited in TAE applications so as to cope with operating condition changes, allowing maximum power point tracking [20]. Should a LA impedance mismatch occur, a fraction of the LA current can be spent in producing a thrust force component proportional to plunger position, resulting in an adjustable electronic stiffness which can tune the LA acoustic impedance and resonance frequency. This however comes at the price of a reduced current margin for active power conversion.

Although the concept was first implemented in wave energy systems [13], the impact of electronic stiffness tuning on power capability limits for a given LA design have not been discussed, and need to be clarified to assess benefits and limits of the technique. Previous work only quantified the ratio of peak to average power under different control strategies [21]. Furthermore, an understanding of electronic stiffness impact on current and voltage limits is

necessary to assess the feasibility of LA designs where physical springs are partially replaced by electronic stiffness. Such a solution can relax mechanical design constraints for springs and LA. Designing springs with high stiffness, extended stroke length and infinite fatigue life is challenging and always results in a larger volume for the spring envelope and complicated layouts with several elements in parallel [22]. In TAE systems, the LA volume has a huge impact on costs because the LA has to be fit into the pressurized vessel, whose wall thickness increases with diameter.

This paper analyses the impact of electronic stiffness on LA power capability and ratings. Two meaningful aspects are considered: firstly the LA power derating caused by the resonance frequency tuning, and secondly the required LA ratings when springs are partially replaced by electronic stiffness. The study is validated with test results on a small LA prototype.

## 2. Background

### 2.1. System layout and equivalent circuit

The power conversion layout for a thermo-acoustic engine coupled to a LA is shown in Fig. 1a. The LA is interfaced to a VSI which operates in regenerative mode. The DC output of VSI is stabilized by a capacitor and can be connected either to a stand-alone load or to a second VSI interfaced to the mains.

The resulting coupled mechanical and electrical equivalent circuit for the TAE-LA-VSI system is shown in Fig. 1b. The TAE is modelled with a force source  $F_e^{j\omega}$  behind the output impedance, which is then lumped with the LA mechanical impedance. Parameters  $m$ ,  $c$ , and  $k$  refer to the equivalent mass, damping and stiffness of the full TAE-LA system.

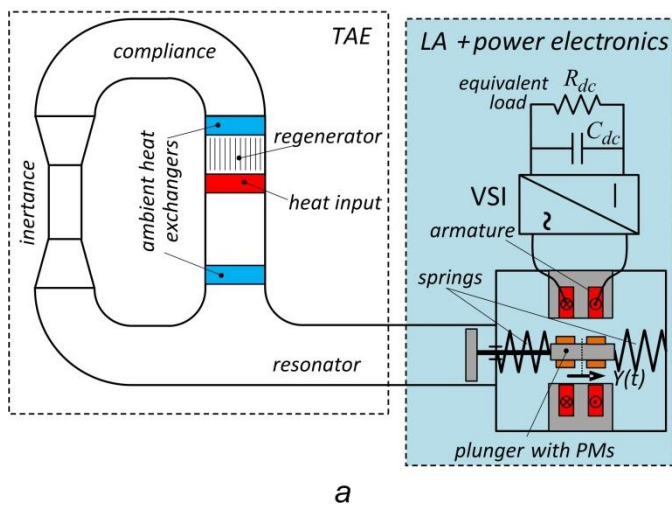


**Fig. 1.** TAE-LA system

- Schematic
- Coupled mechanical-electrical equivalent circuit
- Steady-state phasor diagram and reference frame  $dq$ :  $R$  is neglected

Electromagnetic force  $F_e$  is produced by the interaction between PMs and coil current. Assuming that a fast hysteresis current controller is used, the VSI behaves as a current source instantaneously tracking the reference value set by the controller.

### 2.2. Steady-state operation and rated conditions

Steady-state operation at the generic frequency  $\omega$  is described in terms of phasors by

$$\bar{E} = j\omega k_E \bar{Y} \quad (1)$$

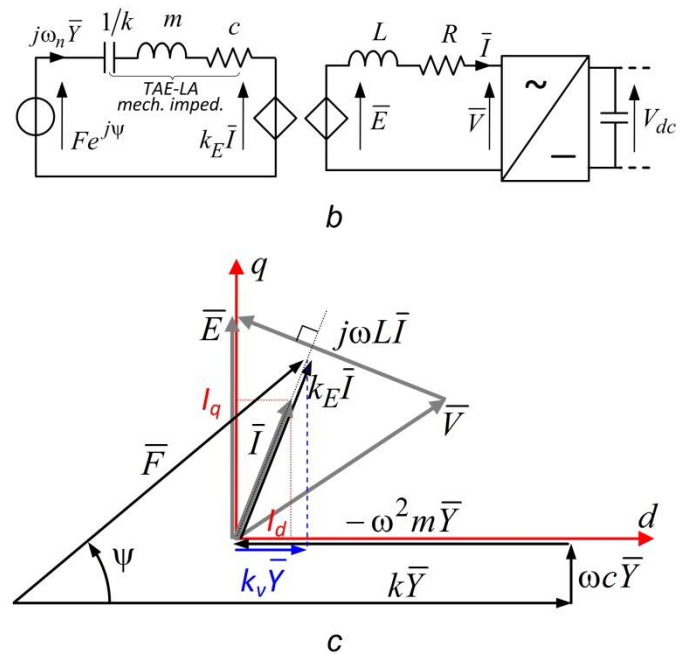
$$(-\omega^2 m + j\omega c + k) \bar{Y} = \bar{F} - k_E \bar{I} \quad (2)$$

$$\bar{V} = \bar{E} - R \bar{I} - j\omega L \bar{I} \cong \bar{E} - j\omega L \bar{I} \quad (3)$$

where the parameters are defined in Fig. 1b. The last equality in (3) neglects the armature resistance  $R$ , as  $R/\omega L$  is generally quite low.

The phasor diagram corresponding to (1)-(3) is shown in Fig. 1c: reference frame  $dq$  has the  $d$ -axis parallel to the displacement phasor  $\bar{Y}$ . Electrical phasors are represented with grey arrows, whereas mechanical phasors are black. Only the quadrature component of current (i.e.  $I_q$ , perpendicular to stroke) is responsible for electromechanical conversion, being in phase with velocity.

When the mechanical and TAE resonance frequencies match, i.e. the equivalent inertia and stiffness forces compensate for each other, the MTPA condition is achieved by controlling armature current so as to have  $I_d=0$  and  $\bar{I}$  in phase with  $\bar{E}$ . This should be considered the reference condition the LA is rated to, and defines the relationships between rated force, current, voltage and stroke. The role of the current component  $I_d$  is discussed in Section 3.



The rated resonance frequency and the critical (base) damping are

$$\omega_{n0} = \sqrt{k/m} \quad , \quad c_{cr} = 2m\omega_{n0} \quad (4a,b)$$

From (2) and (3) at resonance (i.e. when  $\omega = \omega_{n0}$ ) and in MTPA condition (i.e. when  $I_d = 0$ ), relationships between rated EMF,  $E_M$ , current,  $I_M$ , stroke length,  $Y_M$ , and MTPA terminal voltage,  $V_{MTPA}$ , are derived:

$$E_M = \omega_{n0} k_E Y_M \quad (5)$$

$$2\zeta m \omega_{n0}^2 Y_M = F - k_E I_M \quad (6)$$

$$V_M = V_{MTPA} = \sqrt{(k_E \omega_{n0} Y_M)^2 + (\omega_{n0} L I_M)^2} \quad (7)$$

It is convenient to develop the theoretical analysis using dimensionless or per unit (p.u.) stroke length, frequency, damping, current and voltage, according to (8)-(9).

$$y = Y/Y_M \quad , \quad \lambda = \omega/\omega_{n0} \quad , \quad \zeta = c/c_{cr} \quad (8a,b,c)$$

$$i = I/I_M \quad , \quad v = V/E_M \quad (9a,b)$$

In any operating condition, the winding current should not exceed the rated value  $I_M$

$$I_d^2 + I_q^2 \leq I_M^2 \quad \Rightarrow \quad i_d^2 + i_q^2 \leq 1 \quad (10)$$

where  $i_d$  and  $i_q$  are p.u. values.

The required terminal voltage  $V$  depends on the operating conditions

$$V = \sqrt{(\omega k_E Y - \omega L I_d)^2 + (\omega L I_q)^2} \quad (11)$$

Equation (11) also gives the minimum dc-link voltage value to avoid VSI over-modulation and distortion. Some overhead on the value in (11) might be required to guarantee an appropriate margin for dynamic regulation of current. Using p.u. variables, (11) and (7) are translated into

$$v = \sqrt{(\lambda y - \lambda \ell i_d)^2 + (\lambda \ell i_q)^2} \quad , \quad v_M = v_{MTPA} = \sqrt{1 + \ell^2} \quad (12)$$

where  $\ell = \omega_{n0} L I_M / E_M$  is the armature inductance in p.u.

### 3. Electronic stiffness and power capability

The current component  $I_d$  in phase with plunger position can be regulated to produce a force component proportional to plunger position. The effect is equivalent to an “electronic” or “virtual” stiffness  $k_v$  in compliance with Fig. 1c and (13)

$$k_v Y = k_E I_d \quad \Rightarrow \quad k_v = \frac{k_E I_d}{Y} \quad (13)$$

Terms  $I_d$  or  $k_v$  can be either positive or negative:  $k_v$  is capable of changing the overall LA stiffness and resonance

frequency, but it implies a reduction in the available margin for current component  $I_q$  responsible for active power. For a mismatch between resonance frequency  $\omega_{n0}$  and operating frequency  $\omega$ , the ratio  $\lambda$  in (8-b) is no longer unity, and some electronic stiffness  $k_v$  is required to restore resonance conditions according to

$$\sqrt{\frac{k + k_v}{m}} = \omega \quad \Rightarrow \quad \sigma = \frac{k_v}{k} = \lambda^2 - 1 \quad (14a,b)$$

where  $\sigma$  is the electronic to mechanical stiffness ratio. Ratio  $\lambda$  also quantifies the mismatch in the reactive impedance of TAE and LA. From (13)-(14) the required per-unit  $d$ -axis current, assuming operation at rated stroke length, is:

$$i_d = \sigma \frac{k Y_M}{k_E I_M} = (\lambda^2 - 1) \frac{k Y_M}{k_E I_M} \quad (15)$$

A more meaningful formulation of (15) is obtained by neglecting damping force in (6) (i.e. with  $\zeta = 0$ ) and using (6) to express  $k_E$  as a function of thrust force  $F$ , namely:  $k_E \approx F/I_M$ . Also, in rated resonance conditions, stiffness and inertia forces  $k Y_M$  and  $F_m = \omega_{n0}^2 m Y_M$  cancel each other. Thus, (15) becomes:

$$i_d = \sigma \frac{F_m}{F} = (\lambda^2 - 1) \frac{F_m}{F} \quad , \quad F_m = \omega_{n0}^2 m Y_M \quad (16a,b)$$

The maximum p.u.  $q$ -axis current available follows from (10) (treated as an equality) and (16)

$$i_q \cong \sqrt{1 - \left(\frac{F_m}{F}\right)^2 (\lambda^2 - 1)^2} \quad (17)$$

Neglecting losses, the extracted power in p.u. is obtained by multiplying  $i_q$  (17) by  $\lambda$  to account for changes in velocity and EMF. Quantity  $\lambda i_q$  also represents the power derating factor caused by the electronic stiffness.

It is interesting to compare  $\lambda i_q$  to the extracted power  $p_0$  without active tuning (i.e. when  $I_d = 0$ ). In this case, any frequency mismatch produces a drop in the stroke length  $y$ , to be derived from (2) and (6)

$$y = 2\zeta / \sqrt{(1 - \lambda^2)^2 + 4\zeta^2 \lambda^2} \quad (18)$$

The resulting p.u. power  $p_0$  is

$$p_0 = \frac{k_E \omega Y I_M}{E_M I_M} = \lambda y = 2\zeta \lambda / \sqrt{(1 - \lambda^2)^2 + 4\zeta^2 \lambda^2} \quad (19)$$

Quantities  $\lambda i_q$  and  $p_0$  are plotted in Fig. 2a ( $\lambda i_q$  = thin blue lines,  $p_0$  = thick red line):  $p_0$  in (19) is calculated assuming  $\zeta = 5\%$  to include also gas friction effects. The power  $\lambda i_q$  decreases when the ratio of rated inertia force to thrust force  $F_m/F$  increases. For frequency drift above the rated resonance (i.e. for  $\lambda > 1$ ), the LA may convert slightly more power than the rated value, because EMF increases. This

additional power is however likely to be eroded by the rise of stray losses with frequency. For a high ratio  $F_m/F$ ,  $\lambda i_q$  falls sharply and the range for compensable frequency drift narrows. Nevertheless, the  $p_0$  curve is in general much sharper than  $\lambda i_q$  lines. Comparing the power extracted with and without electronic stiffness (thick-red and thin-blue lines respectively) it can be concluded that electronic stiffness is beneficial for inertia force ratios up to  $F_m/F \approx 7$ .

The p.u. terminal voltage is derived by replacing (16) and (17) into (12-a) with  $y=1$  p.u.

$$v = \lambda \sqrt{1 + \ell^2 - 2\ell \frac{F_m}{F} (\lambda^2 - 1)} \quad (20)$$

Fig. 2b shows the p.u. terminal voltage normalized to  $v_{MTPA}$  assuming  $\ell=0.75$  p.u.. The LA operation above resonance corresponds to the field-weakening operation in a rotating PMSM, except that the LA voltage also depends on the stroke length  $y$ , and this feature is absent in a rotating machine. Another peculiarity of the LA is the potential need to operate with negative (magnetizing)  $i_d$ , so as to cope with  $\lambda < 1$ . As shown in Fig. 2b, this results in a higher terminal voltage demand. The terminal voltage may also increase when  $\lambda > 1$ , if the ratio  $F_m/F$  is less than unity, because the effect of a growing  $\lambda$  becomes predominant over field weakening.

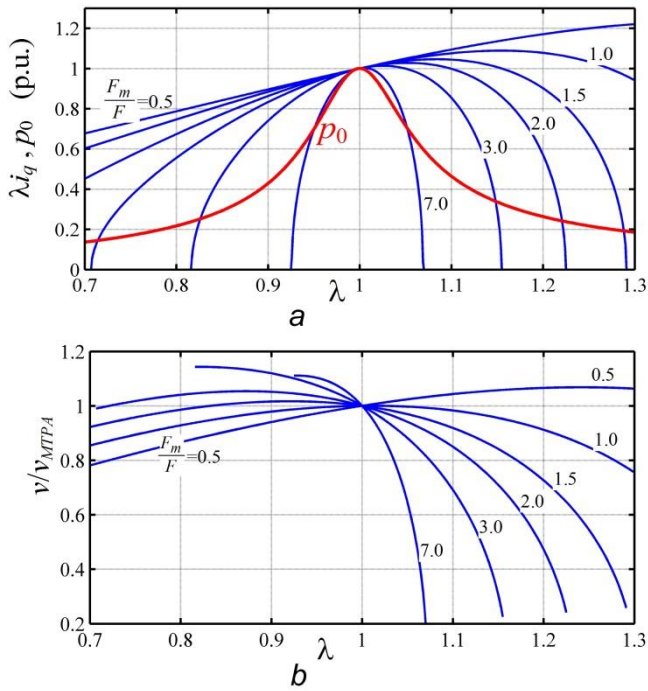


**Fig. 2.** LA characteristics under frequency mismatch using electronic stiffness to restore resonance  
a. Output power derating  
b. Terminal voltage demand (normalized to  $v_{MTPA}$ )

## 4. Required ratings due to Electronic Stiffness

### 4.1. Rationale

Spiral flexure springs are adopted in several linear actuators and LAs [4], as they can provide good plunger and piston alignment with no bearings. However, achieving appropriate axial stiffness and stroke length for resonance frequency in the range 40-100Hz is challenging and calls for large diameters or several springs in parallel [22], which increase the moving mass further. A similar issue has to be faced when using helical springs [3]. The electronic stiffness can be used to supplement or replace mechanical springs in the LA design. This results in a simplified mechanical layout, and potentially more rational use of available LA envelope space. The spring envelope volume is in fact proportional to stored energy,  $kY_M^2$ . If a fraction  $\sigma$  of the required stiffness  $k$  is provided electronically, spring volume decreases proportionally to  $\sigma$ . It is then essential to quantify the current and voltage overrating, due to electronic stiffness implementation.

### 4.2. Theory

The LA design with stiffness entirely supplied by springs is assumed as the reference benchmark, according to (5), (6), (7) and (8). The LA redesign is characterized by a given ratio  $\sigma$ , expressing the fraction of overall stiffness provided electromagnetically by control means instead of using mechanical springs. Power, operating (resonant) frequency and stroke length are the same in the two designs. These parameters are in fact constrained by the optimal acoustic source impedance of the TAE the LA has to work with. The same EMF constant  $k_E$  is assumed for the two LA designs. Rigorously, this last assumption represents a scenario where an existing machine is revamped by replacing part of the springs with electronic stiffness and improving cooling in order to increase current capability. The assumption of unvaried  $k_E$  is also reasonable for a new design, keeping the same magnetic circuit and winding data, and increasing slot space to accommodate larger diameter wires. This might change the slot leakage inductance, but as a first approximation, the total inductance is assumed unvaried.

Fig. 3 compares the electrical phasor diagrams (neglecting stator resistance) in a conventional LA design (left) and in a similar design which provides electronically a fraction  $\sigma$  of the overall stiffness (right).

The p.u. current rating (normalized to the rated current of the benchmark design) accounts for the simultaneous presence of current components  $I_q$  and  $I_d$  which provide the required electromagnetic active force and electronic stiffness. The  $I_q$  component equals the current rating  $I_M$  of the benchmark design, because the two machines must produce the same electromagnetic force. Thus in the new design the p.u.  $q$ -axis current is simply 1 p.u. Also,  $V_M = V_{MTPA}$  is assumed for the benchmark design.

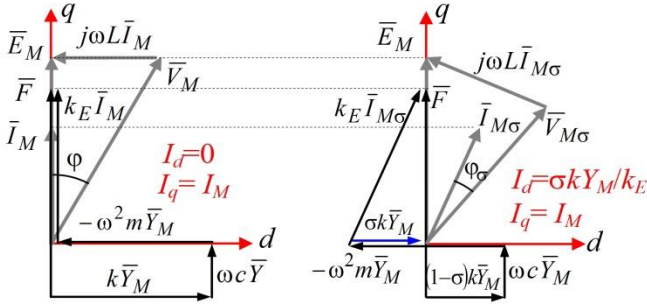


**Fig. 3.** Phasor diagrams in the benchmark design (left) and in the redesign replacing a fraction  $\sigma$  of spring stiffness with electronic stiffness. Resulting resonance frequency and stroke length are unvaried.

Current  $I_d$  is obtained from the electronic stiffness equation

$$k_v Y_M = \sigma k Y_M = k_E I_d \Rightarrow I_d = \frac{\sigma k Y_M}{k_E} \quad (21)$$

The p.u. value of  $I_d$  as a function of  $\sigma$  has already been obtained in the first equality of the left-hand side of (16a). The p.u. value of the required rated current in the LA design using electronic stiffness is then simply  $i_{M\sigma} = (i_d^2 + 1)^{1/2}$ . Using (16), the current rating as a function of  $\sigma$  is

$$i_{M\sigma} = \frac{i_{M\sigma}}{i_M} = \frac{I_{M\sigma}}{I_M} = \sqrt{1 + \sigma^2 \left( \frac{F_m}{F} \right)^2} \quad (22)$$

being by definition  $i_M = 1$  p.u..

As expected, the inertia force plays a crucial role in establishing the current rating: the ratio  $F_m/F$  can be higher than one and depends on the design, especially on rated frequency for the TAE-LA system.

The voltage rating has to be derived from (11) by using rated stroke length and resonant frequency

$$V_{M\sigma}^2 = (E_M - \omega_n L I_d)^2 + (\omega_n L I_M)^2 = V_{MPPA}^2 + (\omega_n L I_d)^2 - 2\omega_n E_M L I_d \quad (23)$$

Dividing (23) by  $E_M^2$  and using p.u. expressions for the inductance  $\ell = \omega_n L I_M / E_M$  and current  $i_d$  (16a) gives

$$v_{M\sigma} = \frac{V_{M\sigma}}{E_M} = \sqrt{1 + \ell^2 + \left( \sigma \ell \frac{F_m}{F} \right)^2 - 2\sigma \ell \frac{F_m}{F}} \quad (24)$$

The resulting expression for  $v_{M\sigma}$  has to be normalized to  $v_M = v_{MTPA}$  (12-b), in order to quantify the voltage overrating with respect to the benchmark design:

$$\frac{v_{M\sigma}}{v_M} = \frac{V_{M\sigma}}{V_{MTPA}} = \sqrt{1 + \sigma^2 \frac{\ell^2}{1 + \ell^2} \left( \frac{F_m}{F} \right)^2 - 2\sigma \frac{\ell}{1 + \ell^2} \frac{F_m}{F}} \quad (25)$$

The new voltage rating is expected to be lower than that of

the benchmark design with no electronic stiffness. In fact, using  $\sigma > 0$  corresponds to operating the LA in the field weakening region.

The bulk capacitor on the dc link is to be sized according to the rated dc voltage and the ripple in the dc current. If the comparison between capacitor requirements in the benchmark and new designs is carried out under the same dc voltage, the overrating for the capacitor ripple current equals the armature current overrating in (22).

The increase in the ratio of peak to average stator power  $\hat{P}/P$  needs to be evaluated when electronic stiffness is used, because this ratio affects the VSI transistor current ratings. As discussed in [21], this ratio is a function of the power factor  $\cos\phi$  at the stator terminals

$$\frac{\hat{P}}{P} = 1 + \frac{1}{\cos\phi} \quad (26)$$

For the benchmark design, the power factor  $\cos\phi$  is simply the ratio  $E_M/V_M = 1/\sqrt{1+\ell^2}$ . As the benchmark and overrated designs have the same average power  $P$ , the power factor  $\cos\phi_\sigma$  in the design with  $\sigma > 0$  is

$$\cos\phi_\sigma = \frac{2P}{V_{M\sigma} I_{M\sigma}} = \frac{V_M I_M}{V_{M\sigma} I_{M\sigma}} \cos\phi \quad (27)$$

Using (22) and (24)-(26) yields:

$$\frac{\hat{P}_\sigma/P}{\hat{P}/P} = \frac{1}{1 + \sqrt{1 + \ell^2}} \left( 1 + \frac{v_{M\sigma} i_{M\sigma}}{v_M i_M} \sqrt{1 + \ell^2} \right) \quad (28)$$

The impact of armature resistance  $R$  deserves some discussion, especially in small LAs. Although  $R$  does not significantly modify the phasor diagram, it causes Joule losses which reduce the power transferred to the dc-link. Calling  $r$  the p.u. value of  $R$  and  $P_{dc} = E_M I_M - R I_M^2$  the dc power extracted by the VSI in the benchmark design, the dc power drop  $\Delta P_{dc\sigma} = R I_d^2$  due to the extra Joule losses caused by  $I_d \neq 0$  is given by

$$\frac{\Delta P_{dc\sigma}}{P_{dc}} = \frac{P_{dc\sigma} - P_{dc}}{P_{dc}} = \sigma^2 \left( \frac{F_m}{F} \right)^2 \frac{r}{1 - r} \quad (29)$$

If needed, (29) can be used to estimate the reduction of  $r$  to be undertaken in the LA redesign in order to limit  $\Delta P_{dc\sigma}$ .

### 4.3. Discussion

Fig. 4a shows the contour lines of the surface  $i_{M\sigma}/i_M = \text{const.}$  in the plane  $(\sigma, F_m/F)$  from (22). In the extreme case where all stiffness is provided electronically (i.e.  $\sigma=1$ ), inertia/thrust force ratios  $F_m/F$  approaching two require about two times the current rating of the benchmark design. Ratio  $i_{M\sigma}/i_M$  also impacts on VSI ratings and gives an estimate of the required increase in copper volume for Joule losses to remain unvaried.

The contour lines of  $v_{M\sigma}/v_M = \text{const.}$  traced in the plane  $(\sigma, F_m/F)$  using (25) are shown in Fig. 4b for two values of the p.u. inductance:  $\ell=0.5$  p.u. (top) and  $\ell=0.75$  p.u.

(bottom). The conclusion anticipated in Section 4.2 is confirmed: the voltage ratio  $v_{M\sigma}/v_M$  tends to be less than unity for values of the p.u. inductance typical of PM machines. In fact, except for very high ratios  $F_m/F$ , the last negative term in the square root of (25) dominates the squared term in the middle. Conversely to what happens with the current rating, electronic stiffness reduces the requirements for rated voltage.

The contour lines of the product apparent power ratio  $(v_{M\sigma}i_{M\sigma}/v_Mi_M)$  can be traced in the plane  $(\sigma, F_m/F)$  combining (22) and (25). The lines are shown in Fig. 4c for the two values of inductance:  $\ell=0.5$  p.u. (top) and  $\ell=0.75$  p.u. (bottom). With an inductance  $\ell$  around 0.5 p.u., and in the worst scenario where  $\sigma=1$ , the product  $(v_{M\sigma}i_{M\sigma})/(v_Mi_M)$  tends to be just less than unity unless the ratio  $F_m/F$  exceeds 2. Between the two 0.95 lines there is a minimum for  $(v_{M\sigma}i_{M\sigma}/v_Mi_M)$ .

If the p.u. inductance  $\ell$  is lower than unity, the square root terms in (28) become very close to one and (28) is well approximated by  $(v_{M\sigma}i_{M\sigma}/v_Mi_M)$ , especially when  $\ell$  is less than 0.5 p.u.. For this reason, Fig. 4c can be considered as also representative of the contour lines of power ratio  $\hat{P}/P$ , and a dedicated figure is not shown here. Higher values of  $\ell$  tend to shift the curves leftwards, increasing the power ratio. It can be concluded that for ordinary values of  $\ell$  there is no significant change in the power ratio  $\hat{P}/P$  for the design with positive electronic stiffness compared to the benchmark design. A different scenario arises if negative stiffness is applied, because in that case the voltage rating increases [21]. In a LA design with reduced amount of mechanical springs, however, electronic stiffness is always positive and substantially higher than zero.

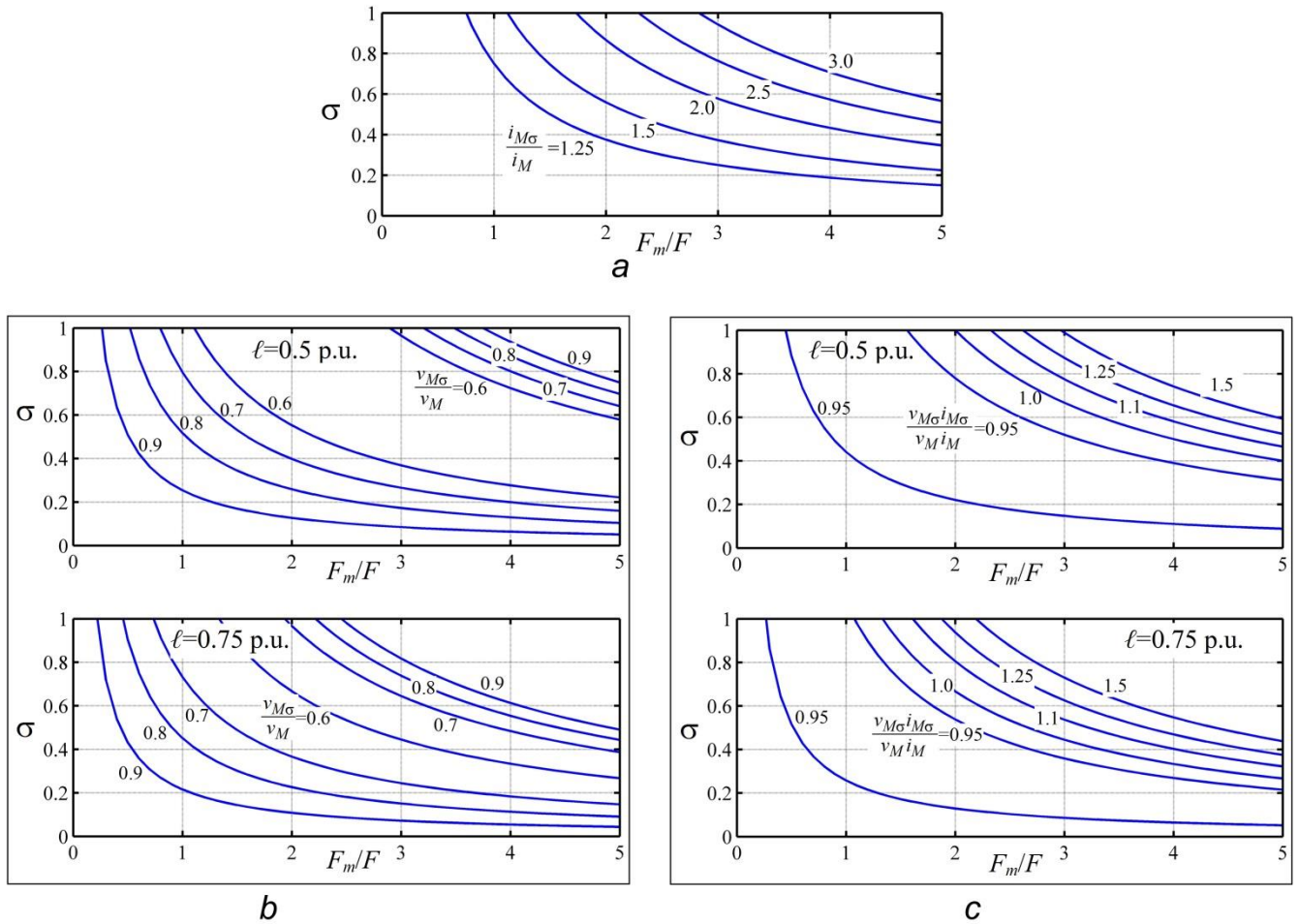


**Fig. 4.** LA characteristics under frequency mismatch using electronic stiffness to restore resonance  
a. Overrating in current  $i_{M\sigma}/i_M$  (22) as a function of  $\sigma$  and  $F_m/F$   
b. Voltage rating ratio  $v_{M\sigma}/v_M$  (25) as a function of  $\sigma$  and  $F_m/F$ ; top:  $\ell=0.5$  p.u.; bottom:  $\ell=0.75$  p.u.  
c. Apparent power ratio  $v_{M\sigma}i_{M\sigma}/v_Mi_M$  combining (22) and (25); top:  $\ell=0.5$  p.u.; bottom:  $\ell=0.75$  p.u..

## 5. Experimental results

The impact of electronic stiffness on LA ratings has been assessed on a small-scale test-rig comprising two identical, rigidly connected 60 W linear machines; one used as a linear motor (LM) the second one operating as a LA. The test-rig is shown in Fig. 5, and ratings of the two machines are detailed in Table 1.

The motor was controlled using a Power Amplifier (PA) and a simple proportional current controller, supplied with a reference signal derived from a function generator, to represent the reference force.

The LA is controlled using a VSI connected to a capacitive dc-link with load resistor and a braking chopper for overvoltage protection. The stroke is measured using a linear variable differential transformer (LVDT), and the electronic stiffness is implemented using analogue techniques: a phase-locked-loop (PLL) generates the necessary reference signals in-phase and in-quadrature with stroke. The stiffness and the  $q$ -axis current responsible for the active power transfer are adjusted with potentiometers. Experimental results are shown in Figs. 6 to 7. As the two machine plungers are coupled together, the actual ratio  $F_m/F$  for the test rig is 1.55 i.e. two times the value of each machine. Current control is implemented by means of a hysteretic comparator.

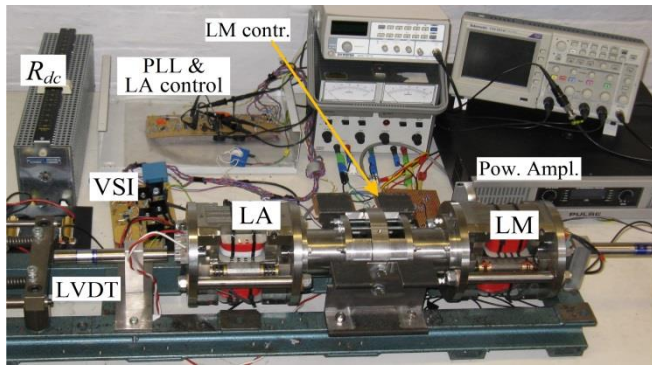


Fig. 5. Test-rig

Table 1 Test Rig Parameters

|                         |               |       |          |
|-------------------------|---------------|-------|----------|
| Armature+VSI resistance | $R$           | 3.3   | $\Omega$ |
| Armature inductance     | $L$           | 0.072 | mH       |
| EMF constant            | $k_E$         | 48.3  | Vs/m     |
| LA Plunger mass         | $m$           | 0.874 | kg       |
| LA Stiffness            | $k$           | 45.3  | kN/m     |
| Rated Stroke (pk)       | $Y_M$         | 3.5   | mm       |
| Rms rated current (pk)  | $I_M$         | 4.23  | A        |
| DC-link rated voltage   | $V_{dc}$      | 100   | V        |
| Rated frequency         | $f_{m0}$      | 36.3  | Hz       |
|                         | $\omega_{m0}$ | 228.1 | rad/s    |
| Force ratio             | $F_m/F$       | 0.774 | -        |

Fig. 6a shows steady-state operation waveforms at the rated resonance frequency of the LA (36.3 Hz). Subplots show stroke, reference currents, actual LA current, PA current and dc-link voltage. The power delivered to the dc-link is about 40 W. The  $d$ -axis reference current is set to zero, not to affect the resonance frequency. Being the power amplifier current proportional to the driving force, the resonance condition is confirmed by zero phase shift between the PA and LA current and by the  $90^\circ$  phase shift between LA current and stroke.

Waveforms in Fig. 6b refer to a test at 40 Hz, corresponding to a frequency drift of 10% above resonance. To make the system resonant at this new frequency, electronic stiffness is introduced resulting in  $I_d = 1.41$  A pk: the value derived from (15) corresponds to 1.38 A pk. The  $90^\circ$  phase shift between stroke and power amplifier current (driving force) proves that resonance conditions have been restored. As a consequence,  $I_d^*$  and  $I_{amp}$  are in phase with each other. The  $q$ -axis reference current is slightly decreased not to violate the rated current constraint.

A further test was conducted at 44 Hz, corresponding to a 21% frequency drift: the waveforms are shown in Fig. 6c. Resonance conditions are restored at this new frequency using electronic stiffness and resulting in  $I_d = 2.80$  A pk which is very close to the theoretical value 2.98 A pk derived from (15). However, there is a significant drop in the dc-link voltage down to 65 V pk, which brings the VSI on the boundary of over-modulation, as shown in the subplot at the bottom. This is due to losses in the LA and VSI which are relatively important in the LA prototype, because of the limited stroke.

Fig. 7 compares power derating factor  $\lambda_{i_q}$  and terminal voltage ratio  $v/v_{MTPA}$  derived from (17) and (20) (continuous line) to the experimental points (markers "o"). Markers "x" denote the squared  $V_{dc}$  normalised to the rated value 100V and represent the actual p.u. dc-power. For frequencies above 45 Hz the dc-link collapses: this is due to stray losses which increase with frequency, in particular eddy-current losses originating in the rotor because of the backward armature field.

In order to investigate the effect of replacing part of the mechanical springs with electronic stiffness, two aligned springs on one side of the LA have been squeezed and clamped by means of metallic brackets so as to reduce the mechanical stiffness to 75% of the original value, resulting in a new resonance frequency of 31.4 Hz (accounting for mass of two plungers). The test-rig is still operated at rated frequency (36.3 Hz), and resonance conditions are restored adding an electronic stiffness equal to 25% of the original total stiffness, i.e.  $k_v = 11.3$  kN/m. This results in  $\sigma = 0.25$  and a theoretical  $d$ -axis current of 1.57 A pk from (20). Fig. 6d presents the steady-state operation waveforms: the resulting  $d$ -axis rotor current is  $I_d = 1.79$  A pk, fairly close to the prediction. To satisfy the current constraint, the  $q$ -axis current is reduced to  $I_q = 3.7$  A pk and this causes a drop in the dc-link voltage to 87 V.

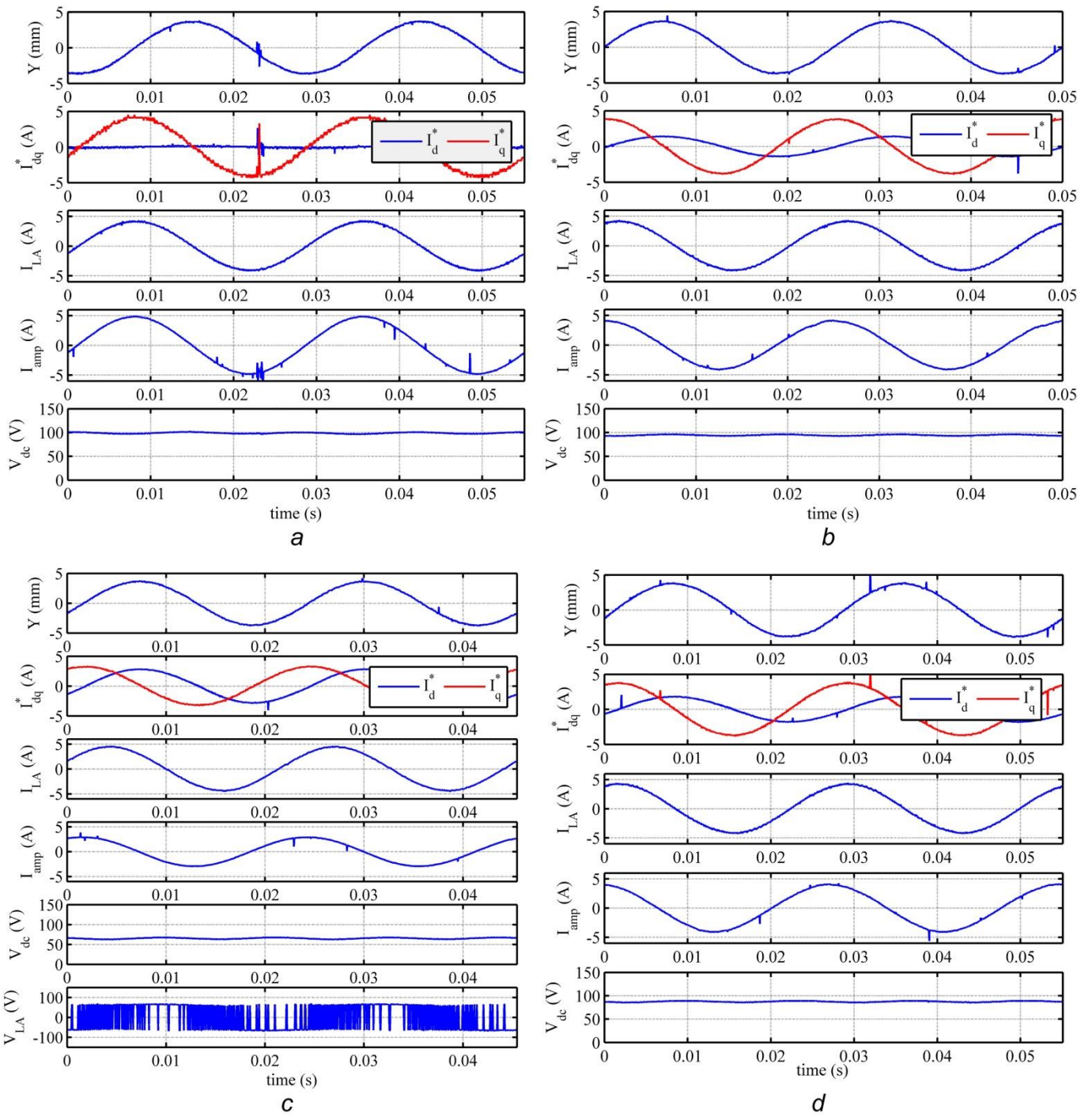


**Fig. 6.** Steady-state experimental waveforms: stroke, reference currents, LA and power amplifier currents and dc-link voltage.

- Test at rated resonance frequency (36.3 Hz) with no electronic stiffness ( $I_d=0$ )
- Test at 40 Hz: resonance restored with electronic stiffness ( $I_d=1.41$  A pk).
- Test at 44 Hz: resonance restored with electronic stiffness ( $I_d=2.82$  A pk), PWM voltage also shown in the last subplot.
- Test at 36.3 Hz with clamped springs: the 25% reduction in mechanical stiffness is compensated for by using electronic stiffness.

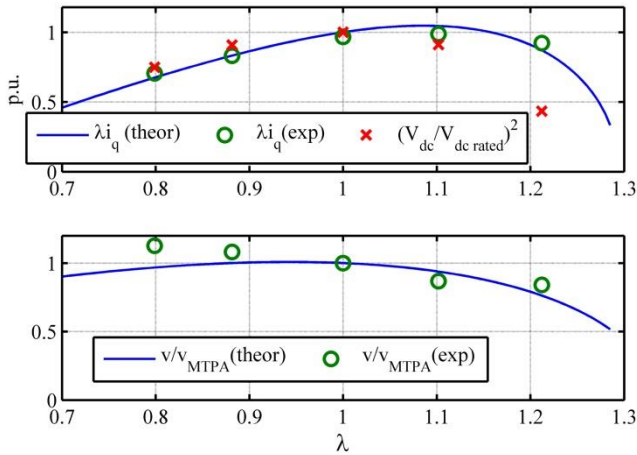


**Fig. 7.** Theoretical and experimental power derating factor and terminal voltage ratio as a function of frequency mismatch  $\lambda$ .

## 6. Conclusion

The design and control of linear alternators for thermoacoustic engines is challenging due to the need to guarantee matching between TAE and LA impedances. The “electronic stiffness” synthesized through the VSI allows the tuning of the reactive component of LA’s mechanical impedance which can then be automatically adjusted to match with the TAE’s counterpart. The TAE-LA system can then be constantly operated at resonance despite TAE frequency drifts and parameter inaccuracies. As shown, the compliance with the constraint for maximum current causes a drop in output power and there is no practical advantage in using electronic stiffness if the ratio inertia to thrust force exceeds seven. By contrast, the rise in the terminal voltage needed to produce negative electronic stiffness is generally limited to a few percent.

Electronic stiffness can also be used to supplement or replace mechanical springs, then easing the mechanical layout of the LA. Analytical expressions for LA ratings are presented for this scenario. An increase in the required rated current is necessary to produce electronic stiffness, and this also impacts on the amplitude of ripple current flowing through the bulk capacitor. Overrating in current depends on the ratio inertia to thrust force on the carriage and appears to be manageable if the force ratio does not exceed 1.5-2. The voltage and ratio peak to average power are not strongly affected by the electronic stiffness.

## 7. References

- [1] G. W. Swift: ‘Thermoacoustic engines’, *J. Acoust. Soc. Am.*, 1998, **84**, (4), pp.1145-1180.
- [2] J. Xia, W. Li, R. Peng, H. Su: ‘Analysis on axial end flux leakage and resonance characteristic of TFPM linear generator for thermoacoustic electric generation system’, *IEEE Trans. Mag.*, 2016, **52**, (12), pp. 1-7.
- [3] Ding Wang, R. Shuttleworth: ‘Linear alternator design for use in heat energy recovery system’, in *6<sup>th</sup> IET PEMD Int. Conf.*, Bristol, UK, 2012.
- [4] Ping Zheng, C. Tong, J. Bai, Bin Yu, Yi Sui, Wei Shi: ‘Electromagnetic design and control strategy of an axially magnetized permanent-magnet linear alternator for free-piston Stirling engines’, *IEEE Trans. Ind. Appl.*, 2012, **48**, (6), pp. 2230-2239.
- [5] J. Wang, M. West, D. Howe, H. Zelaya-De La Parra, W. M. Arshad: ‘Design and verification of a linear permanent magnet generator for free-piston energy converter’, *IEEE Trans. En. Conv.*, 2007, **22**, (2), pp. 299-306.
- [6] A. Sa Jalal, N. J. Baker, D. Wu, ‘Design of tubular Moving Magnet Linear Alternator for use with an External Combustion – Free Piston Engine”, in *8<sup>th</sup> IET PEMD Int. Conf.*, Glasgow, UK, 2016.
- [7] H. Polinder, B. C. Mecrow, A. J. Jack, P. G. Dickinson, M. A. Muller: ‘Conventional and TFPM linear generators for direct-drive wave energy conversion’, *IEEE Trans. En. Conv.*, 2005, **20**, (2), pp. 260-267.
- [8] R. Vermaak, M. J. Kamper: ‘Experimental evaluation and predictive control of an air-cored linear generator for direct-drive wave energy converters’, *IEEE Trans. Ind. Appl.*, 2012, **48**, (6), pp. 1817-1826.
- [9] Zhibin Yu, A. J. Jaworsky, S. Backhaus: ‘Travelling-wave thermoacoustic electricity generator using an ultra-compliant alternator for utilization of low-grade thermal energy’, *Appl. Energy*, 2012, **99**, pp. 135-145.
- [10] Zanxiang Nie, Xi Xiao, R. McMahon, P. Clifton, Yunxiang Wu, S. Shao, ‘Emulation and control methods for direct-drive wave energy converters’, *IEEE Trans. Ind. Inf.*, 2013, **9**, (2), pp. 790-798.
- [11] P. R. M. Brooking, M. A. Mueller: ‘Power conditioning of the output from a linear vernier hybrid permanent magnet generator for use in direct drive wave energy converters’, *IEE Proc. Gener. Transm. Distrib.*, 2005, **152**, (5), pp. 673-681.
- [12] J. K. H. Shek, D. E. Macpherson, M. A. Mueller, J. Xiang: ‘Reaction force control of a linear electrical generator for direct drive wave energy conversion’, *IET Ren. Pow. Gen.*, 2007, **1**, (1), pp. 17-24.
- [13] J. K. H. Shek, D. E. Macpherson, M. A. Mueller: ‘Experimental verification of linear generator control for direct drive wave energy conversion’, *IET Ren. Pow. Gen.*, 2010, **4**, (5), pp. 395-403.
- [14] Feng Wu, Xiao-Ping Zhang, Ping Ju, M. H. Sterling: ‘Modelling and control of AWS-based wave energy conversion system integrated into power grid’, *IEEE Trans. Pow. Syst.*, 2008, **23**, (3), pp. 1196-1204.
- [15] Z. Daboussi: ‘An inverter-based sensorless controller for free-piston Stirling engines’, *35<sup>th</sup> IEEE PESC*, Aachen, Germany, 2004, pp. 1707-1710.
- [16] P. Zheng, Bin. Yu, S. Zhu, Q. Gong, Jiaqi Liu: ‘Research on control strategy of free-piston Stirling-engine linear-generator systems’, *17<sup>th</sup> ICEMS*, Hangzhou, China, 2014, pp. 2300-2304.
- [17] T. M. Lewis, A. von Jouanne, T. K. A. Brekken: ‘Per-unit wave energy converter system analysis’, *2011 IEEE Energy Conversion Congress and Exposition*, Phoenix, AZ, 2011, pp. 4123-4129.
- [18] T. M. Lewis, A. von Jouanne, T. K. A. Brekken: ‘Wave energy converter with wideband power absorption’, *2011 IEEE Energy Conversion Congress and Exposition*, Phoenix, AZ, 2011, pp. 3844-3851.
- [19] K. Wang, J. Zhang, N. Zhang, D. Sun, K. Luo, J. Zou, L. Qiu: ‘Acoustic matching of a traveling-wave thermoacoustic electric generator’, *Applied Thermal Engineering*, 2016, **102**, (5), pp 272-282.
- [20] Min Zangh, M. F. Iacchetti, R. Shuttleworth: ‘Novel Maximum Power Point Tracking Strategies for Electronically-Tuned Linear Alternators’, in *9<sup>th</sup> IET PEMD Int. Conf.*, Liverpool, UK, 2018.

- [21] E. Tedeschi, M. Molinas: 'Impact of control strategies on the rating of electric power take off wave energy conversion' *2010 IEEE International Symposium on Industrial Electronics*, Bari, 2010, pp. 2406-2411.
- [22] N. Chen, X. Chen, Y.N. Wu, C.G. Yang , L. Xu: 'Spiral profile design and parameter analysis of flexure spring', *Cryogenics*, 2006, **46** , (6), pp. 409-419.